Segmentation of High Angular Resolution Diffusion MRI Modeled as a Field of von Mises-Fisher Mixtures

Tim McGraw[1], Baba Vemuri[2], Robert Yezierski[3], and Thomas Mareci[4]

[1] West Virginia University,
Dept. of Computer Science and Electrical Engineering, Morgantown, WV
tmcgraw@csee.wvu.edu
[2] University of Florida,
Dept. of Computer and Information Sciences and Engineering, Gainesville, FL
vemuri@cise.ufl.edu
[3] University of Florida, Dept. of Neuroscience,
Dept. of Orthodontics, Gainesville, FL
ryezierski@dental.ufl.edu
[4] University of Florida, Dept. of Biochemistry,
Gainesville, FL
thmareci@ufl.edu

Abstract. High angular resolution diffusion imaging (HARDI) permits the computation of water molecule displacement probabilities over a sphere of possible displacement directions. This probability is often referred to as the orientation distribution function (ODF). In this paper we present a novel model for the diffusion ODF namely, a mixture of von Mises-Fisher (vMF) distributions. Our model is compact in that it requires very few variables to model complicated ODF geometries which occur specifically in the presence of heterogeneous nerve fiber orientation. We also present a Riemannian geometric framework for computing intrinsic distances, in closed-form, and performing interpolation between ODFs represented by vMF mixtures. As an example, we apply the intrinsic distance within a hidden Markov measure field segmentation scheme. We present results of this segmentation for HARDI images of rat spinal cords – which show distinct regions within both the white and gray matter. It should be noted that such a fine level of parcellation of the gray and white matter cannot be obtained either from contrast MRI scans or Diffusion Tensor MRI scans. We validate the segmentation algorithm by applying it to synthetic data sets where the ground truth is known.

1 Introduction

High angular resolution diffusion imaging (HARDI) has become a popular diffusion imaging mechanism lately in the research communities of MR imaging and analysis. Diffusion tensor models have been used in the past to explain the local geometry of the diffusivity function characterizing the tissue being imaged.

A. Leonardis, H. Bischof, and A. Pinz (Eds.): ECCV 2006, Part III, LNCS 3953, pp. 463–475, 2006.

A diffuson tensor model primarily assumes a single dominant direction of diffusion and hence is well suited for modeling tissue that exhibits unidirectional diffusivity behavior. In general however, more general mathematical models are needed to represent the diffusivity function which may exhibit X-shaped local geometry corresponding to crossing fibers or bifurcating fibers. The DTI model is well known for its deficiency in coping with such complex local geometries and HARDI is one way to overcome this problem. Several research articles have been published that describe techniques for processing HARDI data sets. For example, Tuch [1, 2] developed the HARDI acquisition and processing and later Frank [3] used the spherical harmonics expansion of the HARDI data to characterize the local geometry of the diffusivity profiles. Neither one of these methods address the issue of segmenting the field of probability distributions. A level-set approach to segmenting HARDI data has been given by Jonasson et al. [4].

Several research groups have actively pursued the problem of segmenting DTI data sets. Some have used scalar-valued maps computed from DTI and applied standard level-set based scalar image segmentation methods to them [5] while, Feddern et al., [6] extended the geodesic active contour model to accomodate tensor field segmentation. A region-based active contour was used with a Frobenius norm based tensor distance in Wang et. al., [7] and Rousson et. al., [8] developed an extension of the classical surface evolution scheme by incorporating region based statistics computed from the tensor field. Recently, Wang et. al., [9, 10] introduced an affine invariant tensor dissimilarity and used it to reformulate the active contour implementation of the Mumford-Shah piecewise constant version [11] and the piecewise smooth version [12] of the segmentation model to suit tensor field segmentation. The piecewise constant DTI segmentation model was generalized by Lenglet et al. [13] to the case of regions with piecewise constant non-unit variances.

Since HARDI data have the ability to resolve fiber crossings, it would be natural to expect a better parcellation of the fiber connectivity pattern than that obtained using DTI. In this paper, we will present results on synthetic data sets that will demonstrate the truth of this hypothesis. We will also present segmentation results on real HARDI data acquired from a rat spinal cord. These results were visually validated, but quantitative validation of real data segmentation will be the focus of future work.

2 Modeling Diffusion

In DTI, data are modeled in terms of the diffusion tensor. The apparent diffusion coefficient is a quadratic form involving the tensor, and the diffusion displacement pdf is a Gaussian with covariance matrix equal to a constant multiple of the inverse of the tensor. For HARDI, we will model neither the diffusivity nor the displacement pdf, but will instead model the diffusion ODF.

In order to design efficient algorithms, we wish to find a continuous parametric model for the ODF with a small number of parameters, which is capable of describing diffusion in the presence of intravoxel orientational heterogeneity.

To put our proposed model in perspective we will first review some models for diffusion used in previous literature.

Gaussian mixture models (GMM) are one of the most commonly used models for multimodal distributions. The GMM is a convex combination of Gaussian density functions, $N(\mathbf{x}|\mu_i, \Sigma_i)$. Each Gaussian component is characterized by a 3×3 covariance matrix, Σ_i, which has 6 independent elements. For diffusion data, all components have a mean $\mu = 0$.

The GMM, $P(\mathbf{x}) = \sum_{i=1}^{m} w_i N(\mathbf{x}|\mu_i, \Sigma_i)$, where m is the number of components in the mixture, can describe the 3-dimensional diffusion displacement pdf. Each Gaussian component has its own 3×3 covariance matrix, Σ_i, which will have 6 independent elements. For diffusion data, all components will have $\mu_i = 0$.

However, we are primarily concerned with the directional characteristics of diffusion. This can be characterized by the marginal distribution, $P(\theta, \phi)$ obtained by integrating over the radial component of $P(\mathbf{x})$. Additionally, with the GMM, we must be careful to impose the positive-definiteness constraint on the covariance matrix of each component of the mixture. Previously Fletcher and Joshi [14] have described geodesic analysis on the space of diffusion tensors. The analysis includes an algorithm for computing the intrinsic mean of diffusion tensors. Later in this paper we will describe a similar analysis on the space of ODFs which will result in much simpler algorithms.

The spherical harmonic (SH) expansion is a useful representation for complex-valued functions on the sphere. We can represent the diffusion with the expansion $d(\theta, \phi) = \sum_{l=0}^{L} \sum_{m=-l}^{l} a_{l,m} Y_{l,m}(\theta, \phi)$, where $Y_{l,m}$ are the spherical harmonic basis functions. Note that the coefficients $a_{l,m}$ are complex-valued, so that the storage requirement is double that of an equivalent model with real variables, and the arithmetic operations are more costly as well. Frank [15] suggests an expansion truncated at order $L = 4$ (or higher) to describe multiple fiber diffusion. This requires at least 15 complex-valued coefficients per voxel. In general, the order L expansion can describe diffusion with $L/2$ fiber directions. Özarslan [16] has developed an extremely fast algorithm for computing a SH expansion for the ODF given a SH expansion of the diffusivity. Chen et al. [17] have previously presented a technique for estimating a regularized field of apparent diffusion coefficient (ADC) profiles as a SH expansion.

The diffusion tensor imaging model described previously represents diffusion using a rank-2 tensor. Diffusion has been described more generally by Özarslan et al. [18, 19] by considering tensors of higher rank. A cartesian tensor of rank I will, in general, have 3^I components. Due to symmetry, the number of distinct components in a high rank diffusion tensor will be much smaller. By generalizing the concept of trace, it is possible to quantify the anisotropy of diffusion described by tensors of arbitrary rank [20].

Since tensors of odd rank imply negative diffusion coefficients, only even rank tensors are appropriate for describing diffusion. For diffusion tensors of rank 4,6, and 8, the number of distinct components are 15, 28, and 45 respectively. It is not clear how to extract fiber directions from higher rank tensors.

2.1 von Mises-Fisher Mixture Model

Many statistical approaches involve data over $\Re^n$. Since we are dealing with multivariate data over the sphere, S^2, we wish to express the data using distributions over this domain. Distributions over spherical domains are discussed in detail by Mardia and Jupp [21].

In this section we will present a directional model for the ODF in terms of von Mises-Fisher distributions. This model has fewer variables than the previously discussed models, allows the fiber directions to be extracted easily, involves constraints which are simpler to satisfy, and leads to a closed-form for several useful measures. The von Mises distribution over the circle can be generalized

Fig. 1. Example vMF distributions ($\kappa = 1, 5, 15, 25$) with same mean direction, μ

to spheres of arbitrary geometry by keeping the log of the distribution linear in the random variable $\mathbf{x}$ as in

$$M_p(\mathbf{x}|\mu,\kappa) = \left(\frac{\kappa}{2}\right)^{p/2-1} \frac{1}{2\pi\Gamma(p/2)I_{p/2-1}(\kappa)} \exp(\kappa\mu^T\mathbf{x}) \tag{1}$$

where $|\mathbf{x}| = 1$ and $|\mu| = 1$, κ is the concentration parameter and I_k denotes the modified Bessel function of the first kind, order k. The concentration parameter, κ, quantifies how tightly the function is distributed around the mean direction μ. For $\kappa = 0$ the distribution is uniform over the sphere. The distributions are unimodal and rotationally symmetric around the direction μ.

For $p = 3$ the distribution is called the von Mises-Fisher (vMF) distribution, and can be written

$$M_3(\mathbf{x}|\mu,\kappa) = \frac{\kappa}{4\pi\sinh(\kappa)} \exp(\kappa\mu^T\mathbf{x}). \tag{2}$$

A useful characteristic of the vMF distribution is that the product of two vMFs may also be written as an unnormalized vMF. Since

$$\exp(\kappa_i\mu_i^T\mathbf{x}) \exp(\kappa_j\mu_j^T\mathbf{x}) = \exp((\kappa_i\mu_i + \kappa_j\mu_j)^T\mathbf{x}) \tag{3}$$

we have

$$M_3(\mathbf{x}|\mu_i,\kappa_i)M_3(\mathbf{x}|\mu_j,\kappa_j) \propto M_3(\mathbf{x}|(\frac{\kappa_i\mu_i + \kappa_j\mu_j}{\rho(\kappa_i,\kappa_j,\mu_i,\mu_j)}), \rho(\kappa_i,\kappa_j,\mu_i,\mu_j)),$$
$$\rho(\kappa_i,\kappa_j,\mu_i,\mu_j) = \sqrt{\kappa_i^2 + \kappa_j^2 + 2\kappa_i\kappa_j(\mu_i \cdot \mu_j)}. \tag{4}$$

Since the vMF distribution is unimodal, we require a combination of these distributions to represent a general ODF. In fact, since the ODF is antipodally

symmetric, we will need a mixture to describe diffusion in even a single fiber region. Since the antipodal pair have $\mu_1 = -\mu_2$, we can specify a mixture with only 3 variables per component: the two spherical coordinate angles describing μ, and κ. The general ODF will have the form

$$ODF(\mathbf{x}) = \sum_{i=1}^{m} w_i M_3(\mathbf{x}|\mu_i, \kappa_i) \tag{5}$$

where m is the number of components in the mixture. Choosing a convex combination of vMF distributions, the weights have the property $\sum_{i=1}^{m} w_i = 1$ and $w_i \geq 0$. This ensures that the mixture still has nonnegative probabilities, and will integrate to 1. Since vMF distributions obey the property (3), the product of two von Mises-Fisher mixture models is also proportional to a vMF mixture model.

It can also be shown [22] that the Renyi entropy (order α) of the vMF mixture has closed form (for certain values of α). This is useful since the entropy of the mixture model can be used as measure of anisotropy. It can also be shown, using property (3), that there is a closed-form equation for the L_2 distance between two vMF mixtures.

2.2 Fitting the vMF Mixture

In this section we describe a nonlinear least-squares technique for computing the vMF mixture model. We will assume that we have been given a discrete set of samples of the ODF. We seek a mixture of vMFs which agrees with these samples in the least-squares sense while obeying the constraints imposed on the vMF parameters.

Using the spherical coordinates $\mathbf{x} = [\cos\theta \sin\phi, \sin\theta \sin\phi, \cos\phi]^T$ and $\mu = [\cos\alpha \sin\beta, \sin\alpha \sin\beta, \cos\beta]^T$, we may write the vMF in polar form:

$$M_3(\theta, \phi|\alpha, \beta, \kappa) = \frac{\kappa}{4\pi \sinh(\kappa)} \exp(\kappa[\cos\phi \cos\beta + \sin\phi \sin\beta \cos(\theta - \alpha)]) \tag{6}$$

The energy function we will seek to minimize is

$$\begin{aligned} \min_{w,\kappa,\mu} \sum_{i=1}^{N} [p(x_i) - \sum_{j=1}^{m/2} \frac{w_j}{2} (M(x_i|\kappa_j, \mu_j) + M(x_i|\kappa_j, -\mu_j))]^2 \\ -\gamma_1 \sum_{j=1}^{m/2} \log(w_j) + \gamma_2 (1 - \sum_{j=1}^{m/2} w_j)^2 - \gamma_3 \sum_{j=1}^{m/2} \log(\kappa_j) \end{aligned} \tag{7}$$

where the first term is the least-squares error. Note that we are fitting the data, $p(\mathbf{x})$, to a mixture of $m/2$ antipodal vMF pairs. The second term, with weight γ_1, is a barrier function which constrains the weights, w_j, to be greater than zero. The third term, with weight γ_2, constrains the sum of the weights to be 1. The fourth term, with weight γ_3, is a barrier function which constrains the

concentration parameters, κ_j, to be greater than zero. Equation (7) is solved using Levenberg-Marquardt.

It is likely that most voxels will fit a mixture of 4 vMF pairs (4 fiber orientations per voxel) quite well. In this case the mixture of 8 vMF distributions requires only 15 real-valued parameters to completely describe due to pairwise antipodal symmetry. Once we have fit the vMF mixture to the ODF, we can directly extract the fiber directions, $\{\mu\}$.

3 The Space of vMF Distributions

The von Mises-Fisher distribution is parameterized by two variables: the concentration parameter $\kappa \in \Re^+$ and $\mu \in S^2$. For each point in $\Re^+ \times S^2$ there is a corresponding vMF distribution. The curved geometry of this space of vMF distributions will influence how we formulate distances, geodesics, interpolation functions and means. A general treatment of the geometry of the spaces formed by parametric distributions is given by Amari [23, 24].

3.1 Riemannian Geometry

The space of vMF distributions forms a differentiable manifold, a space which locally behaves like Euclidean space. A Riemannian manifold is a smooth manifold supplied with a Riemannian metric. This metric takes the form of an inner product, $\langle v, w \rangle_p$ defined on the tangent space, T_pM, for each point, p, on the manifold, M. The Riemannian metric allows us to measure the length of a curve, $\gamma(t)$ between two points, p, q on M.

$$L(\gamma) = \int_p^q (\langle \gamma'(t), \gamma'(t) \rangle_{\gamma(t)})^{\frac{1}{2}} dt \tag{8}$$

We will see how the notions of metric, distance, geodesics, interpolation and mean are all related. The mean can be defined in terms of the distance, d, as the point, μ, which satisfies

$$\min_{\mu \in M} \sum_{i=1}^{N} d^2(\mu, x_i). \tag{9}$$

Interpolation can be defined in terms of a weighted mean, so we can interpolate between the distributions p, q by minimizing

$$\min_{\mu \in M} t d(\mu, p) + (1-t) d(\mu, q). \tag{10}$$

3.2 Riemannian Exp and Log Maps

Let M be some manifold, and T_pM be the tangent space at $p \in M$. Consider all geodesics going through the point, p, on M. Given a tangent vector, $v \in T_pM$, it is known that there is a unique geodesic, γ, such that $\gamma(0) = p$, and $\gamma'(0) = v$.

If the manifold is geodesically complete, as it is in our case, the Riemannian exponential map, $\mathrm{Exp}_p : T_pM \rightarrow M$, can be defined as $\mathrm{Exp}_p(v) = \gamma(1)$.

The Riemannian log map is the inverse of the exponential map, $\mathrm{Log}_p : M \rightarrow T_pM$. This map only exists in the region near p where the Exp map is invertible. If the log map, Log_p exists at q, we can write the Riemannian distance between p and q as $d(p,q) = ||\,\mathrm{Log}_p(q)||_p$.

3.3 Overview of the Geodesic Analysis

In this section we will give a brief overview of the geodesic analysis of the space of vMF mixtures. The complete analysis is given by McGraw [22]. Similar analysis has been presented by Fletcher and Joshi [14] for the space of diffusion tensors, and by Fletcher et al. [25] for the space of shapes represented by medial atoms. An outline of our analysis is given below:

1. Show that $\Re^+$ and S^2 are symmetric spaces.
2. Show that $M = \Re^+ \times S^2$ is a symmetric space.
3. Find a transitive Lie group action on M.
4. Formulate arbitrary geodesics on M by applying the Lie group action to a known geodesic.
5. Formulate the Exp and Log maps for M.

A symmetric space [26] is a connected Riemannian manifold such that at each point on the manifold there exists a distance preserving mapping which reverses geodesics through that point. Such a mapping can be computed for the spaces $\Re^+$ and S^2. It can also be shown that the direct product of symmetric spaces is also a symmetric space.

Now we can consider a vMF distribution to be a point in a symmetric space. If M_1 and M_2 are two metric spaces and $x_1, y_1 \in M_1$ and $x_2, y_2 \in M_2$, then the metric for $M_1 \times M_2$ is $d((x_1,x_2),(y_1,y_2))^2 = d(x_1,y_1)^2 + d(x_2,y_2)^2$. This result allows us to formulate distances between vMF distributions in terms of distances on the spaces $\Re^+$ and S^2.

The action of group G on M is called transitive if for any two $x, y \in M$ there exists a $g \in G$ such that $g \cdot x = y$. If the group action is transitive then M can be shown to be a homogeneous space, and the action of G does not change distances on $M : d(g \cdot p, g \cdot q) = d(p,q)$. Geodesics on a homogeneous space can then be computed by applying the group action to other geodesics.

3.4 Exp and Log Maps for vMF Distributions

We have used the fact that the direct product of symmetric spaces is also a symmetric space to deduce that the space of vMF distributions is symmetric. Now we will use this fact to compute the Exp map for vMFs. For spaces which are expressed as direct products, we can write the exponential map as the direct product of the exponential maps for the constituent spaces. For a single vMF, let $p = (\kappa, \mu)$ represent the distribution $M_3(\mathbf{x}|\kappa,\mu)$, and $v = (a,u) \in T_pM$ be the tangent vector. Then

$$\mathrm{Exp}_p(v) = \left(\kappa \exp(a), Q \begin{bmatrix} u_x \frac{\sin||u||}{||u||} \\ u_y \frac{\sin||u||}{||u||} \\ \cos||u|| \end{bmatrix} \right)^T \tag{11}$$

where Q is the orthogonal matrix which transforms μ to $[0, 0, 1]^T$. The distance between vMFs can be written using the Log maps as

$$d((\kappa_i, \mu_i), (\kappa_j, \mu_j)) = \sqrt{\log(\frac{\kappa_j}{\kappa_i})^2 + (\cos^{-1}(\mu_i \cdot \mu_j))^2}. \tag{12}$$

An example of interpolation between two vMF distributions computed using the Exp and Log maps is shown in Figure 2.

(a) $\gamma(0)$ (b) $\gamma(0.25)$ (c) $\gamma(0.5)$ (d) $\gamma(0.75)$ (e) $\gamma(1)$

Fig. 2. Points along the geodesic between two vMF distributions

4 The Space of vMF Mixtures

Now, let us investigate the space of mixtures of vMF distributions. The mixture model of m components is given in Equation (5). At first, it may seem that we can simply extend the results of the previous section, and consider these mixtures to come from the space $(\Re^+ \times \Re^+ \times S^2)^m$. However, considering the set of weights as an point in $(\Re^+)^m$ ignores the convexity constraint on the weights. The space $(\Re^+)^m$ includes linear combinations of vMFs whose weights do not sum to 1.

Instead, we consider the square roots of the weights, $\{\sqrt{w_1}...\sqrt{w_m}\}$. The convexity constraint now becomes $\sum_{i=1}^{m} \sqrt{w_i}^2 = 1$ with $w_i >= 0$. So, we can consider the space of the square roots of the weights to be a hypersphere, S^{m-1}. Then, the space of mixtures with m components is $S^{m-1} \times (\Re^+ \times S^2)^m$.

4.1 Exp and Log Maps for the Space of vMF Mixtures

For the vMF mixture, the exponential map is the direct product of the exponential maps for each vMF, and the exponential map for S^{m-1}. Since we are quite unlikely to have more than 4 fiber orientations present within a single voxel, we will consider further the case of mixtures having 8 antipodal pairs, or 4 independent weights. In this case, the space of the square roots of $\{w\}$ is the unit hypersphere S^3. Fortunately, the space S^3 is well studied, since this is equivalent to the space of unit quaternions. In fact, S^3 forms a Lie group with respect to the quaternion multiplication operator.

The exponential map for S^3 is

$$\mathrm{Exp}_p(v) = \left(\frac{\sin(\frac{1}{2}||v||)}{||v||} v, \cos(\frac{1}{2}||v||) \right)^T \tag{13}$$

and the log map is given by

$$\mathrm{Log}_p(q) = \frac{2\cos^{-1}(q_w)}{|q_{vec}|} q_{vec} \tag{14}$$

where q_{vec} and q_w are the vector and scalar parts respectively of the quaternion q. We may now simply extend the results of the previous section to formulate the distance between mixtures. An example of interpolation between mixtures is shown in Figure 3.

(a) $\gamma(0)$ (b) $\gamma(0.25)$ (c) $\gamma(0.5)$ (d) $\gamma(0.75)$ (e) $\gamma(1)$

Fig. 3. Points along the geodesic between two vMF mixtures

Previously, the intrinsic mean problem has been solved with a gradient descent algorithm [27, 25, 28]. The gradient of the energy function in Equation (9) can be written in terms of the Log map. The algorithm, as given by Fletcher and Joshi [25] is

Given: $x_1, ..., x_N \in M$
Find: $\mu \in M$, the intrinsic mean
$\mu_0 = x_1$
repeat
  $\Delta\mu = \frac{\tau}{N} \sum_{i=1}^{N} \mathrm{Log}_{\mu_t}(x_i)$
  $\mu_{t+1} = \mathrm{Exp}_{\mu_j}(\Delta\mu)$
until $||\Delta\mu|| < \epsilon$

5 Application to Segmentation

The mean and distance formulations discussed in the previous section can be quite useful in the context of model-based segmentation. In this section we will present results obtained using the hidden Markov measure field (HMMF) model, though the model we have developed may be used with many other segmentation schemes. This method, presented by Marroquin et al. [29], is a variation on the Markov random field segmentation model, but has fewer variables and can solved without slow stochastic methods. We use the gradient projection Newtonian descent algorithm for finding the resulting optimization problem.

5.1 Results

The proposed vMF fitting technique was applied to a synthetic dataset. This data simulated anisotropic Gaussian diffusion in a medium with a single dominant orientation. The orientation varies spatially according to a sinusoidal function. The result of the fitting is shown in Figure 4. The angular difference between the known dominant orientation and the mean direction, μ, of the dominant vMF component was computed at each voxel. The average angular error was 0.026 degrees. The results of the HMMF segmentation using the geodesic distance applied to synthetic HARDI data are presented below. The first two datasets are piecewise constant vMF fields with two regions. The results are presented in Figure 5a and b. Figure 5a shows the segmentation obtained from a field where the two regions differ in direction. In Figure 5b, the regions differ only in the concentration parameter, κ. There are no classification errors. In Figure 5c the results for segmentation of vMF mixtures is shown. The data consists of several piecewise constant areas and a crossing. Here the algorithm has correctly segmented each region and the crossing.

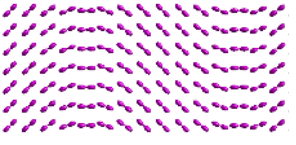

Fig. 4. vMF model fit to synthetic data

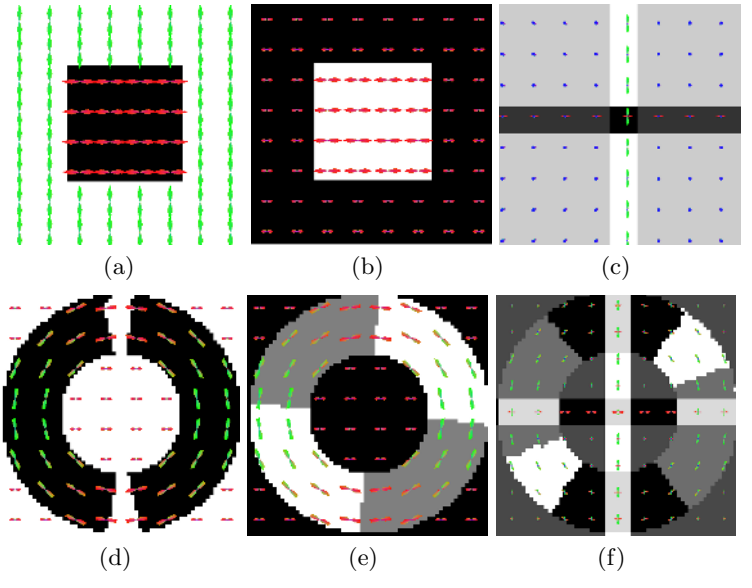

Fig. 5. HMMF segmentation of synthetic data

Next the algorithm was tested on curved regions. A synthetic dataset consisting of a circular region with vMFs oriented tangentially was created. A two region segmentation was computed in Figure 5d, and a three phase segmentation was computed in Figure 5e. Note that the two phase segmentation has identified nearly the entire circular region, even though the segmentation model is piecewise constant. Three regions was sufficient to segment the entire circular region.

The algorithm was then tested on a dataset with curved geometry and crossings. The results are shown in Figure 5f. In this case, the algorithm was able to discriminate between adjacent regions with multiple directions.

Finally the algorithm was applied to the lumbar region of a rat spinal cord. The data were acquired at the McKnight Brain Institute on a 14.1 Tesla Bruker Avance Imaging system with a diffusion weighted spin echo pulse sequence. Imaging parameters were : effective TR = 2000 ms, $\Delta = 17.5$ ms, $\delta = 1.5$ ms. Diffusion-weighted images were acquired with 46 different gradient directions with $b = 1500$ and a single image was acquired with $b \approx 0$. The image field of view was 60 x 60 x 300 μm^3, and the acquisition matrix was 72 x 72 x 40.

The RMS difference between the vMF model and a 6th order spherical harmonic expansion of the ODF are shown in Table (1). The spherical harmonic expansion was computed using the diffusion orientation transformation described by Özarslan et al. [16]. The RMS differences were computed for real and synthetic data in regions with one and two fibers per voxel. The single-fiber synthetic data show the best fitting results. The single and double-fiber fitting errors for the real data are comparable.

Table 1. RMS fitting error between vMF model and 6th order SH expansion

	Single Fiber	Double Fiber
Synthetic Data	0.0003	0.0013
Real Data	0.0018	0.0022

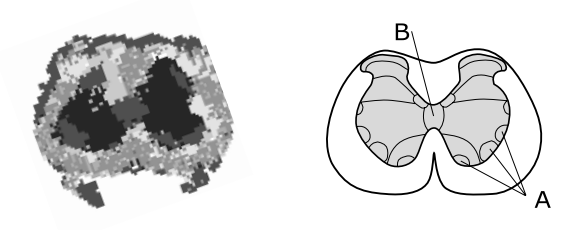

Fig. 6. Segmentation of spinal cord dataset (left) and anatomy from atlas (right)

The results of the segmentation are shown in the left side of Figure 6. The anatomical atlas shown in the right side of Figure 6 shows the the gray matter and white matter in an axial slice of the lumbar region of the spinal cord in gray and white respectively. Several of the distinct regions of the gray matter we would like to be able to segment are depicted in this image. Due to the low resolution of the data, we are unable to segment some of the finer structures.

We are, however, able to distinguish the lateral motor neurons (labeled A in the atlas) and the dorsal gray commissure (labeled B in the atlas) from the remainder of the gray matter.

6 Conclusion

We have introduced a novel model for orientational diffusion with mixtures of von Mises-Fisher distributions. This model leads to closed-form expressions for distances and anisotropy measures. A geodesic framework for working with this model was also presented. The results were applied within the hidden Markov measure field segmentation framework, and the results were presented for synthetic and real data. The technique was able to distinguish between regions of gray matter in the rat spinal cord which correspond to known anatomy.

Acknowledgements

This research was supported in part by the grant NIH-NS42075 and by Siemens Corporate Research (Princeton, NJ). We wish to thank Sara Berens and Evren Özarslan for the spinal cord data.

References

1. Tuch, D.S., Weisskoff, R.M., Belliveau, J.W., Wedeen, V.J.: High angular resolution diffusion imaging of the human brain. In: Proc. of the 7th Annual Meeting of ISMRM, Philadelphia, PA (1999) 321
2. Tuch, D.S., Reese, T.G., Wiegell, M.R., Wedeen, V.J.: Diffusion MRI of complex neural architecture. Neuron **40** (2003) 885–895
3. Frank, L.R.: Characterization of anisotropy in high angular resolution diffusion-weighted MRI. Magn. Reson. Med. **47** (2002) 1083–1099
4. Jonasson, L., Hagmann, P., Bresson, X., Thiran, J.P., Wedeen, V.J.: Representing diffusion mri in 5d for segmentation of white matter tracts with a level set method. In: IPMI. (2005) 311–320
5. Zhukov, L., Museth, K., Breen, D., Whitaker, R., Barr, A.: Level set modeling and segmentation of DT-MRI brain data. J. Electronic Imaging **12** (2003)
6. Feddern, C., Weickert, J., Burgeth, B.: Level-set methods for tensor-valued images. In: Proc. Second IEEE Workshop on Geometric and Level Set Methods in Computer Vision. (2003) 65–72
7. Wang, Z., Vemuri, B.C.: Tensor field segmentation using region based active contour model. In: ECCV (4). (2004) 304–315
8. Rousson, M., Lenglet, C., Deriche, R.: Level set and region based surface propagation for diffusion tensor mri segmentation. In: ECCV Workshops CVAMIA and MMBIA. (2004) 123–134
9. Wang, Z., Vemuri, B.C.: An affine invariant tensor dissimilarity measure and its applications to tensor-valued image segmentation. In: CVPR (1). (2004) 228–233
10. Wang, Z., Vemuri, B.C.: DTI segmentation using an information theoretic tensor dissimilarity measure. IEEE Trans. Med. Imaging **24** (2005) 1267–1277

11. Chan, T.F., Vese, L.A.: A level set algorithm for minimizing the mumford-shah functional in image processing. In: VLSM '01: Proceedings of the IEEE Workshop on Variational and Level Set Methods (VLSM'01), Washington, DC, USA, IEEE Computer Society Press, New York (2001) 161–170
12. Tsai, A., Yezzi, A., Willsky, A.: Curve evolution implementation of the Mumford-Shah functional for image segmentation, denoising, interpolation, and magnification. Volume 10. (2001) 1169–1186
13. Lenglet, C., Rousson, M., Deriche, R., Faugeras, O.D., Lehericy, S., Ugurbil, K.: A Riemannian approach to diffusion tensor images segmentation. In: IPMI. (2005) 591–602
14. Fletcher, P.T., Joshi, S.C.: Principal geodesic analysis on symmetric spaces: Statistics of diffusion tensors. In: ECCV Workshops CVAMIA and MMBIA. (2004) 87–98
15. Frank, L.R.: Anisotropy in high angular resolution diffusion-weighted MRI. Magn. Reson. Med. **45** (2001) 935–939
16. Özarslan, E., Shepherd, T., Vemuri, B.C., Blackband, S., Mareci, T.: Resolution of complex tissue microarchitecture using the diffusion orientation transform. Technical report, (University of Florida)
17. Chen, Y., Guo, W., Zeng, Q., Yan, X., Huang, F., Zhang, H., He, G., Vemuri, B.C., Liu, Y.: Estimation, smoothing, and characterization of apparent diffusion coefficient profiles from high angular resolution DWI. In: CVPR (1). (2004) 588–593
18. Özarslan, E., Mareci, T.H.: Generalized diffusion tensor imaging and analytical relationships between diffusion tensor imaging and high angular resolution diffusion imaging. Magn. Reson. Med. **50** (2003) 955–965
19. Özarslan, E., Vemuri, B.C., Mareci, T.: Fiber orientation mapping using generalized diffusion tensor imaging. In: IEEE Symp. on Biomedical Imaging (ISBI), Washington DC (2004) 1036–1038
20. Özarslan, E., Vemuri, B.C., Mareci, T.H.: Generalized scalar measures for diffusion MRI using trace, variance and entropy. Magn. Reson. Med. **53** (2005) 866–876
21. Mardia, K.V., Jupp, P.: Directional Statistics. 2nd edn. John Wiley and Sons Ltd., New York (2000)
22. McGraw, T.: Denoising, Segmentation and Visualization of Diffusion Weighted MRI. PhD dissertation, University of Florida, Gainesville, FL (2005)
23. Amari, S.: Information geometry on hierarchy of probability distributions. IEEE Trans. Information Theory **47** (2001) 1701–1711
24. Amari, S., Nagaoka, H.: Methods of information geometry. AMS, Providence, RI (2000)
25. Fletcher, P.T., Lu, C., Pizer, S.M., Joshi, S.: Principal geodesic analysis for the study of nonlinear statistics of shape. IEEE Transactions on Medical Imaging **23** (2004) 995–1005
26. Klingenberg, W.: Riemannian Geometry. de Gruyter, Berlin (1982)
27. Pennec, X., Fillard, P., Ayache, N.: A Riemannian framework for tensor computing. International Journal of Computer Vision **65** (2005) to appear
28. Karcher, H.: Riemannian center of mass and mollifier smoothing. Comm. Pure Appl. Math. **30** (1977) 509–541
29. Marroquin, J.L., Santana, E.A., Botello, S.: Hidden Markov measure field models for image segmentation. IEEE Trans. Pattern Anal. Mach. Intell. **25** (2003) 1380–1387